IEEE Access
Multidisciplinary | Rapid Review | Open Access Journal

Received February 4, 2021, accepted February 28, 2021, date of publication March 2, 2021, date of current version March 15, 2021.

Digital Object Identifier 10.1109/ACCESS.2021.3063630

Metamaterial-Based Antenna Performance Enhancement for MIMO System Applications

HEDI SAKLI[1,2], C. ABDELHAMID[1], C. ESSID[3], AND N. SAKLI[2]
[1]MACS Laboratory, National Engineering School of Gabes, University of Gabes, Gabes 6029, Tunisia
[2]EITA Consulting, 78360 Montesson, France
[3]SERCOM Laboratory, Tunisia Polytechnic School, University of Carthage, La Marsa 2078, Tunisia

Corresponding author: Hedi Sakli (hedi.s@eitaconsulting.fr)

ABSTRACT This paper presents a method for designing a new two-element ultra-wideband (UWB) multiple-input-multiple-output (MIMO) antenna. We propose the design of an ultra-wideband antenna has been proposed with a study of its properties. An isolation technique using well-designed metamaterials is presented to achieve the miniaturization and performance of the two antennas and ensure proper operation of the MIMO system with a very small spacing between radiating elements ($\lambda/12$) where λ is the length waves in a vacuum. The metamaterials used considerably reduce the coupling of multi-antennas. The application of these materials called split-ring resonator (SRR) on the antenna patch plane has contributed to the increase in the performance of the antenna studied in terms of S parameters, multiplexing efficiency, diversity gain (DG), radiation properties and envelope correlation coefficient (ECC). This increases the transmission rate. This antenna system offers advantages such as reduction in weight and bulk, which facilitates its integration into a receiver, dedicated to 5G and connected objects.

INDEX TERMS Diversity Gain, ECC, metamaterials, mutual coupling, UWB-MIMO antenna.

I. INTRODUCTION

This Consumer mobile communications, downloading videos and using mobile applications account for the bulk of the current use of radio resources in 4G networks; but for the spectrum of uses and the diversity of users to be greatly expanded, [1]–[3], many research efforts and many proposals are beginning to emerge for the implementation of a new standard called 5G, which targets very diverse sectors which are important pillars of a society: energy, health, media, industry or transport.

The choice of the operating frequency band depends essentially on the intended application [4]–[6]. For applications in space and in microwave imaging for detection through obstacles, ultra-wideband seems to be the most suitable since improving the resolution in distance necessarily requires broadening the bandwidth. We can therefore conclude that a better resolution is obtained for a wider bandwidth. According to [7]–[9], a fractional bandwidth of more than 100% can significantly reduce the level of side lobes and significantly improve the resolution in scattered gratings. Therefore, for microwave imaging applications with the UWB MIMO radar system, it is necessary to transmit the signal over a sufficient bandwidth [10]. The development of an antenna network can be divided into three outcomes: selection of the elementary antenna, selection of the network topology and the study of the coupling between the elements of the network [11]–[13]. The antenna, being the crucial device in wireless communication, must not limit the transmission or reception of data and must meet many requirements and constraints. For UWB antennas, the task becomes more complicated, or they must be delicately designed to have good characteristics in a wide operational bandwidth [14], [15].

Known by the acronym UWB, Ultra-Wide Band describes a much older technology with a modern name. It has been named by different names such as pulse technology, carrier less technology.... Many UWB bands of MIMO antennas have been studied in the literature [16]–[24]. Indeed, it dates back to the last years of the 19th century but it does not recognize any development because of the problems linked to the creation of interferences with other systems as well as the possibility of the implementation of these impulse systems was not still approvable. It is since the 1960s of the 20th centuries that researchers have been focusing on the study and development of these systems and initially allow their use in military applications and the United States Department of Defense (DoD). In the 90s, the advancement of this technology accelerated and over time it regained considerable interest and was the subject of several works which pushed it to commercial use Converging services and systems to

The associate editor coordinating the review of this manuscript and approving it for publication was Kuang Zhang.

TABLE 1. Basic microstrip line parameters.

parameters	w	h	ε_r	t
values	3.02 mm	1.6 mm	4.4	0.035mm

full integration on a single small platform often requires the design of compact ULB antennas to accomplish multiple tasks.

In this paper, we propose a UWB antenna operating in the [2]–[18] GHz band with a gain between 2 and 6.5 dB and efficiency greater than 70%. A good agreement between the simulations and the measurements of the reflection parameter S11 at the input of the antenna is obtained. Next, we propose a MIMO system with two very close antennas spaced at λ/12. The insertion of 5 SRR cells suitably designed and arranged linearly between the two radiating elements allows us to reduce the effect of mutual coupling down to −35 dB at the 7.8 GHz frequency with an isolation gain of −20 dB compared to that of two antennas without SRR. In this paper a comparison between simulations and measurements of the transmission parameter S21 is presented. This shows that the proposed UWB-MIMO multi-antenna system represents a good candidate for wireless communications systems such as 5G and connected objects.

II. DESIGN OF NEW MULTIFUNCTION PATCH ANTENNA

The antenna model developed within the framework of this study is based on a square monopole fed by a power line with partial ground plane and characteristic impedance 50Ω. A microstrip line is connected directly to a patch where the junction point is on the axis of symmetry of the patch. In order to adapt the antenna to its feed, the width of this line is evaluated based on the equation 1 below [25]. The characteristic impedance of the microstrip line depends on the line width, the height and the permittivity of the substrate according to the equation (1)

$$Z_c = \frac{120\pi}{\sqrt{\varepsilon_{eff}}\left[\frac{w}{h} + 1.393 + 0.667\ln\left(\frac{w}{h} + 1.444\right)\right]} \quad (1)$$

With ε_{eff} represents the effective permittivity of the substrate, h the height of the dielectric substrate and w the width of the line. The values of the parameters set and calculated for the microstrip line are given in Table 1.

Figure 1 represents the reflection and transmission coefficient of the 50 Ohms microstrip line. A reflection coefficient less than −16 dB is obtained in the [0.1-40] GHz band with a transmission coefficient greater than −1 dB in the same frequency band.

The dimensions of the rectangular patch can be obtained from the analytical expressions given in [25] by

$$L = \frac{c}{2f\sqrt{\varepsilon_{eff}}} - 2\Delta L \quad (2)$$

$$\Delta L = 0.412h\frac{\left(\varepsilon_{eff}+0.3\right)\left(\frac{w}{h}+0.262\right)}{\left(\varepsilon_{eff}-0.258\right)\left(\frac{w}{h}+0.813\right)} \quad (3)$$

$$\varepsilon_{eff} = \frac{\varepsilon_{r+1}}{2} + \frac{\varepsilon_r - 1}{2}\left(1 + \frac{10h}{w}\right)^{\frac{-1}{2}} \quad (4)$$

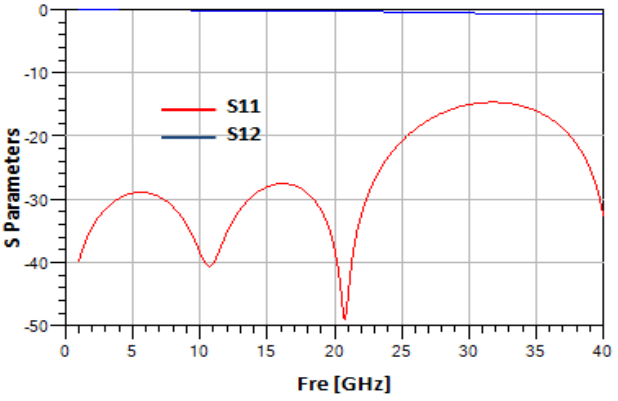

FIGURE 1. Simulation of the reflection and transmission coefficients of the 50 Ohms microstrip line.

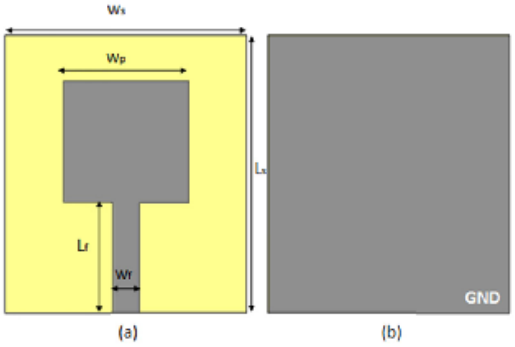

FIGURE 2. Structure of the basic antenna: (a) the radiating element, (b) the ground plane.

The initial width of the antenna is given by the following expression [26]

$$w = \frac{\lambda_0}{2}\left(\frac{\varepsilon_r}{2}\right)^{\frac{-1}{2}} \quad (5)$$

c it is the speed of light in the air; f is the frequency; L is the resonant length of the patch; w is its width; h is the thickness of the substrate; ε_r is its effective permittivity of the medium. The substrate used is a dielectric of the FR4-epoxy type (relative permittivity $\varepsilon_r = 4.4$; substrate thickness hs = 1.6 mm and loss tangent tg (δ) = 0.02). Figure 2 shows the initial antenna composed of a square patch of side wp = 14.5 mm. The variation of the reflection coefficient S_{11} at the input of the rectangular antenna as a function of the frequency in the band [2]–[18] GHz is shown in figure 3. A narrow band is obtained for our initial antenna.

The most commonly used bandwidth broadening techniques are successively the reduction of the quality factor Q, the introduction of multiple resonances and the impedance matching technique that we have applied in this paper. The techniques used are based on the insertion of slits or notches which allow to modify the paths of the surface currents and therefore of the impedance distribution along the antenna. This method is interesting since it allows to keep or even reduce the size of the original antenna which will not compromise its networking.

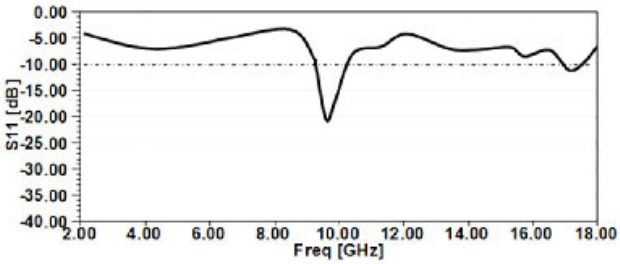

FIGURE 3. Reflection coefficient as a function of the frequencies of the basic square antenna.

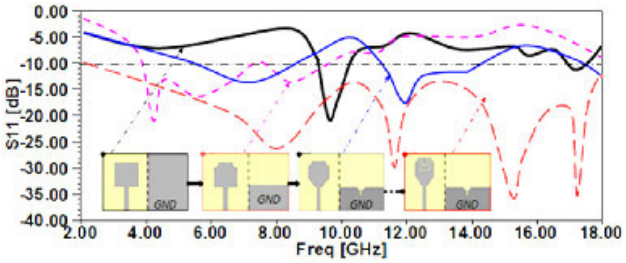

FIGURE 4. Reflection coefficient of the base antenna, of the studied antennas without and with modifications to the ground plane and optimized final antenna.

To overcome the problem of its narrow bandwidth as illustrated in FIG. 3, we apply a certain number of modifications to it. The proposed antenna consists of a modified square patch and a partial ground plane separated by a dielectric substrate of the FR4 epoxy type, with a permittivity equal to 4.4 and a thickness hs = 1.6 mm. A triangular opening at the level of the ground plane with a rectangular notch as shown in figure 4. This antenna is fed by a microstrip line of characteristic impedance equal to 50 Ω. Figure 4 shows the effect of changes in the ground plane on the reflection coefficient. We can see an improvement in terms of adaptation after the addition of the rectangular slots, with a minimum value of around −33 dB and a considerable decrease in the level of the S_{11} by making the U-slot while expanding the bandwidth. The U-slot antenna with notches in the ground plane provides a signal less than −10 dB in a bandwidth that spans from 2.18 GHz to 18 GHz with a relative band of over 140%. This is our proposed antenna.

Figure 5 illustrates the final proposed antenna. The optimal parameters obtained by simulation are summarized in Table 2.

Figure 6 shows the simulation results of the evolution of the real and imaginary parts of the antenna impedance as a function of the frequency. We notice that the impedance has good adaptability: in most of the required frequency bands the real part changes around 50 Ω and in most of the frequency band the imaginary part is around 0 Ω.

Figure 7 shows the variation of the gain of the entire antenna as a function of the frequency in the desired band. The maximum gain value obtained is approximately 6.5 dB, and its minimum value is 1.43 dB for the frequency of 2 GHz.

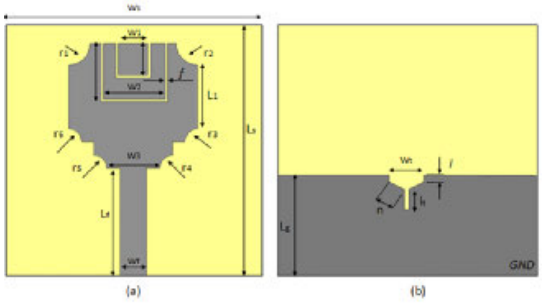

FIGURE 5. The proposed antenna: (a) front view, (b) bottom view.

TABLE 2. Optimized dimensions of the proposed antenna.

components	Parameters	Values (mm)
Dielectric substrate	Ws	25
	Ls	30
	εr	4.4
	Hs	1.6
Ground plan	Lg	12.5
	Wt	3.5
	N	2.4
	I	0.75
	Lt	2.3
Patch	r1=r2	2.5
	W1	3.4
	L1	7.5
	r3=r4=r5=r6	1.5
	W3	6.17
	Lf	13.5
	Wf	3
	W2	7.2
	F	0.3

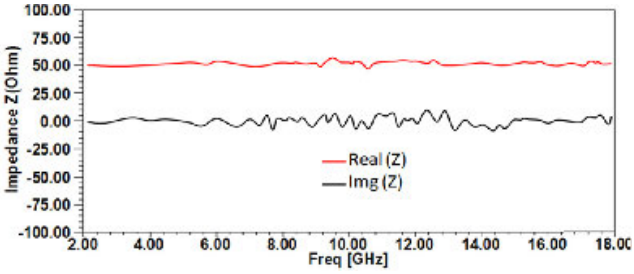

FIGURE 6. Input impedance of the proposed antenna.

Figure 8 shows the radiation patterns of our proposed antenna in polar representation for the frequencies 7.8 GHz and 15.3 GHz in the H plane (XZ plane: Phi = 0 °) and the E plane (YZ plane: Phi = 90 °). This antenna has a quasi-omnidirectional radiation which is relatively stable throughout the operating band.

Figure 9 shows that the efficiency of the monopoly antenna is high. Its value exceeds 80% in the operating band.

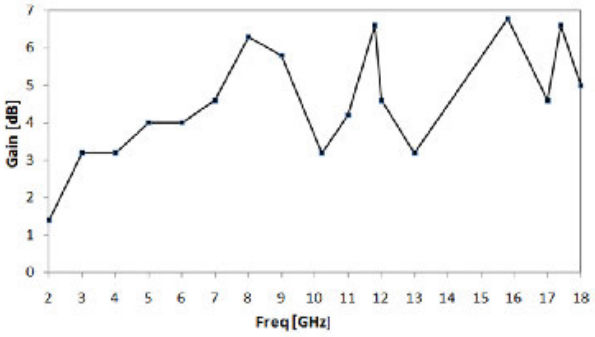

FIGURE 7. The change in gain as a function of frequency.

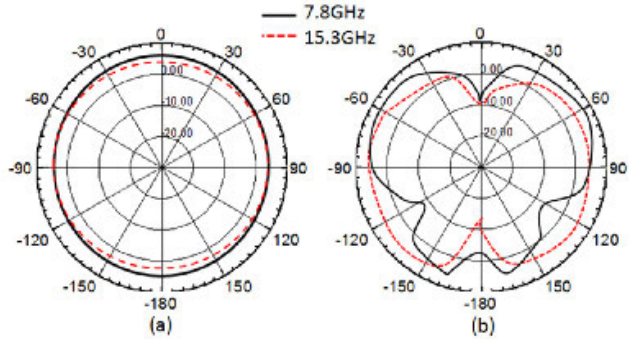

FIGURE 8. Antenna radiation pattern for different frequencies: (a) E plane and (b) H plane.

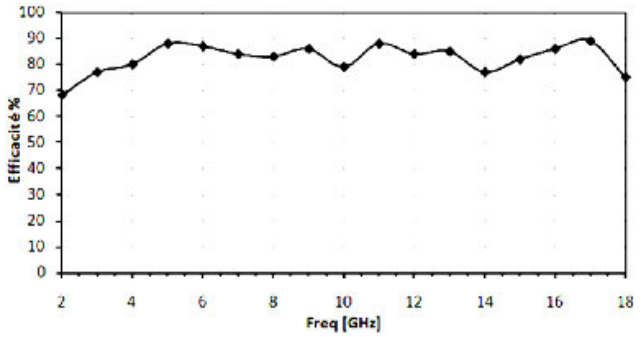

FIGURE 9. Efficiency of the proposed antenna.

This means that almost the majority of the energy injected into the antenna is radiated.

Note also that the current distributions of this antenna for several frequencies are shown in Figure 10. We notice that an additional path for the surface current has been created with the presence of the slits. This leads to produce another resonance and consequently increase the bandwidth [26].

A prototype of this antenna was made for the purpose of comparison (see figure 11). The comparison of the simulation results and those of the measurement concerning the reflection coefficient are presented in figure 12.

The reflection coefficient S_{11} of the proposed antenna as a function of the frequency obtained with simulation as well as the measurement results are illustrated in figure 12. It is noted that the measurement results are in good agreement with those of the simulation in most cases of the operating band.

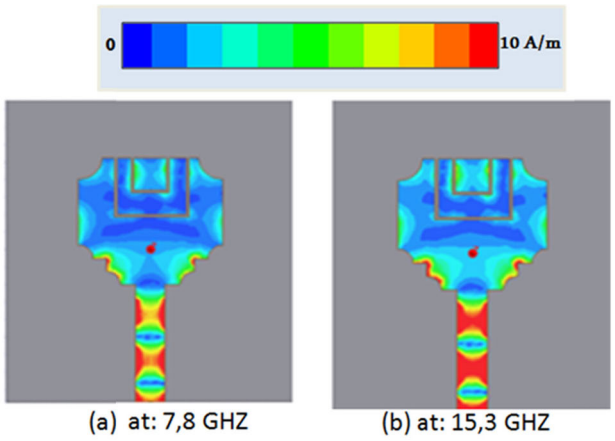

FIGURE 10. Current distribution of the proposed antenna for different frequencies: (a) at 7.8 GHz, (b) at 15.3 GHz.

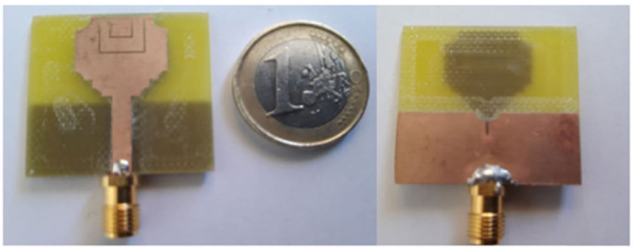

FIGURE 11. Prototype of the proposed antenna.

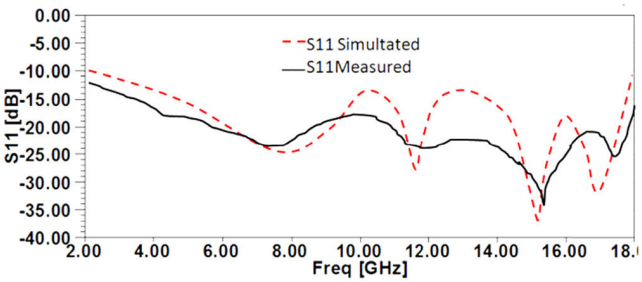

FIGURE 12. Reflection coefficient of the proposed antenna.

Note that the small difference observed between the experimental results and those of the simulation is mainly due to manufacturing tolerances and measurement errors.

The antenna was put in an anechoic chamber (see figure 13) in order to measure its radiation. Figure 14 shows the radiation pattern of this antenna simulated and measured at the frequency 7.8 GHz in the H plane. It is noted that there is a concordance between the measurement and the simulation.

III. STUDY OF THE CHARACTERISTICS OF A MIMO SYSTEM WITH TWO ANTENNAS

In this section, an isolation technique based on the insertion of a metamaterial, consisting of a periodic structure composed of 5 SRRs, will be applied to an antenna system composed of two elements in order to ensure an increase in 'insulation at 15 dB. For this, a single band antenna system dedicated to UWB coverage will be developed. This system is of the

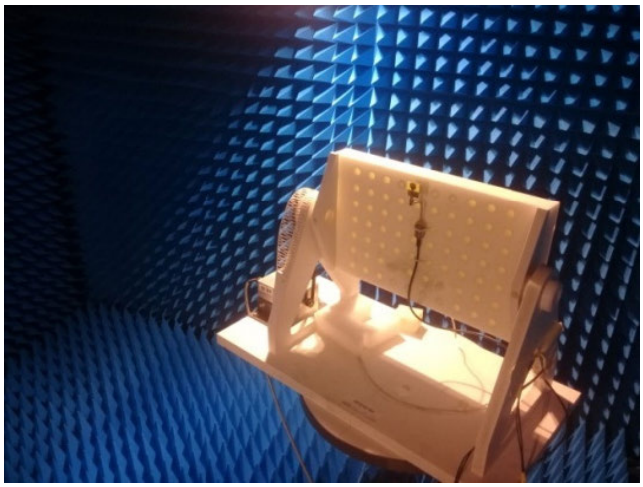

FIGURE 13. Device for measuring the antenna in the anechoic chamber.

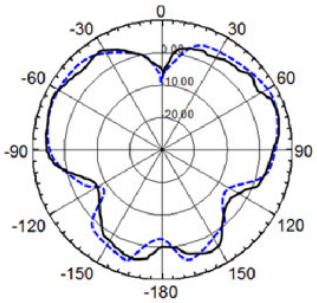

FIGURE 14. Simulated and measured radiation pattern of the proposed antenna at the 7.8 GHz frequency in the H plane.

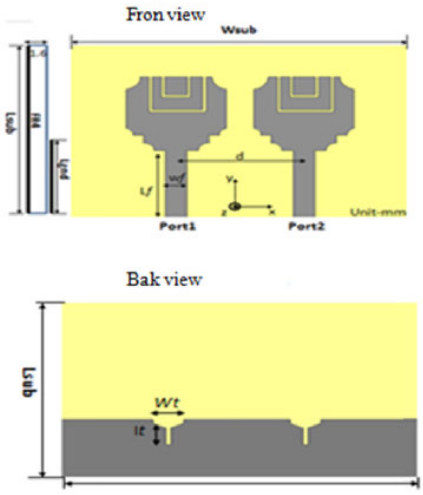

FIGURE 15. Geometry of the UWB-MIMO antenna system: front view and bak view.

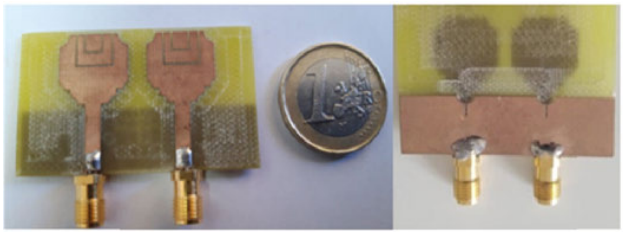

FIGURE 16. Prototype of the MIMO antenna in figure 15.

massive MIMO type with 2 elements. It is necessary to have two power ports. To do this, we first designed a reference system made up of two ULB antennas. Figure 15 illustrates the geometry of two identical MIMO-UWB antenna elements initially proposed in Figure 5, which are placed on a PCB of dimensions Wsub × lsub = 48 x 35 mm2. The distance between the two elements (center to center) is noted d = 16.8 mm. A partially truncated shared ground plane is implemented and placed at the rear of the substrate, which guarantees good impedance matching over a wide range of frequencies. The parameters of antenna 1 are optimized in terms of reflection coefficient. Thanks to a parametric study, we obtain the following values: Wsub = 48 mm, Lsub = 35 mm, Lgnd = 12.5 mm, Lf = 13.5 mm. Figure 16 shows the prototype of the manufactured antenna system.

The simulated and measured S parameters $|S_{11}|$ and $|S_{21}|$ antenna 1 (antenna 2 is suitable for 50 Ohms) are shown in figures 17.a and 17.b respectively. They are in reasonable agreement, while the difference between them around 2.1 GHz is mainly due to the effects of losses due to the measuring cable. An important feature is that this antenna can operate from 2 to 18 GHz (including ISM 2.45 GHz and UWB bands) for $|S_{11}|$ and $|S_{21}| < -10$ dB. However, the isolation is very close to −10 dB at lower frequencies (due to the electrically smaller separation); which is not sufficient for many applications. Normally, isolation greater than 15 dB is required. Further improvements are therefore necessary. The separation of the two elements is a critical parameter to obtain good impedance matching and better insulation. The simulated reflection coefficients | S11 | and the mutual coupling coefficients | S21 | with different values of d (from 18 to 32 mm) are obtained and represented respectively in figures 18.a and 18.b. From figure 18.a, we Note that the bandwidth is sensitive to the separation of the two antenna elements. The effects on the mutual coupling coefficients | S21 | are relatively small as shown in figure 18.b. It can be seen that the Smaller coupling is obtained with the greatest separation (d is 32mm) on a UWB, but it cannot meet UWB operation requirements and maintain small overall size for the MIMO antenna.

To better understand the mutual coupling between the two antennas due to the smallness of space between them, it is preferable to study these interferences, due to radiation in the near field, by analyzing the current distributions on the two elements. The simulated current distributions of antenna 1 at frequencies 7.8 and 15.3 GHz are shown in Figures 19.a and 19.b respectively. When port 1 is energized, port 2 terminates with a 50 Ω load. It can be seen that the surface current in the orifice of the excited element1 induces currents in the second element at all frequencies through the common ground plane. For MIMO antennas to work well they must be independent with a minimum of coupling; so better isolation is needed.

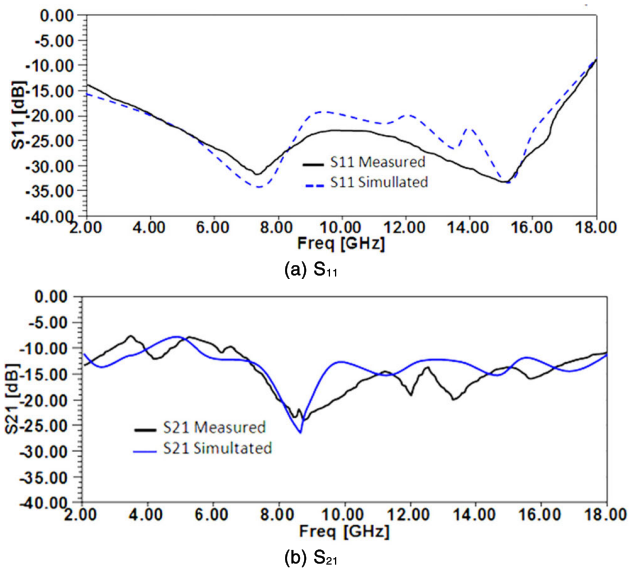

FIGURE 17. Simulated and measured S-parameters of antenna 1.

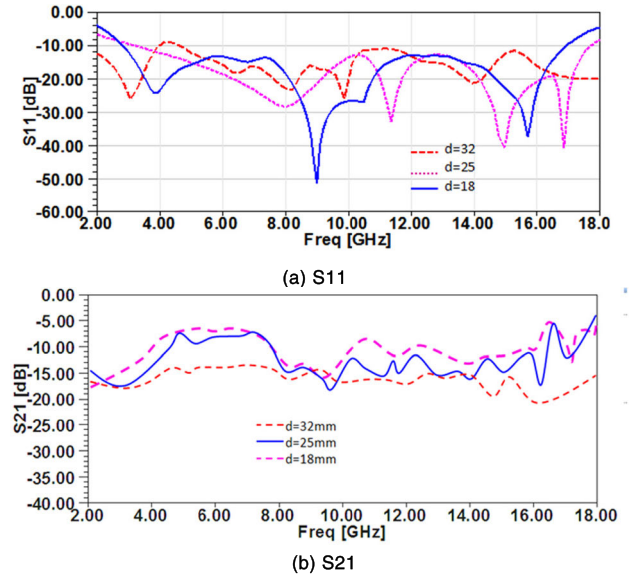

FIGURE 18. Simulated S parameters: (a) S11 reflection coefficient. (b) transmission coefficient S21.

A simple and effective approach is to work on the common ground plane to limit the flow of current from one port to the other, ultimately reducing the mutual coupling between the two ports.

IV. REDUCTION OF MUTUAL COUPLING BASED ON METAMATERIALS

To solve the isolation problem, we propose the installation of a new structure of metamaterials between the two antennas, which is constituted by a linear array of 5 identical unit cells of the SRR type (see figure 20). The edge-to-edge separation between the two radiating elements is maintained at 0.073 λ (2.8 mm) at 7.8 GHz.

The geometry and dimensions of the SRR are described in figure 21. The resonator is made of copper deposited on a

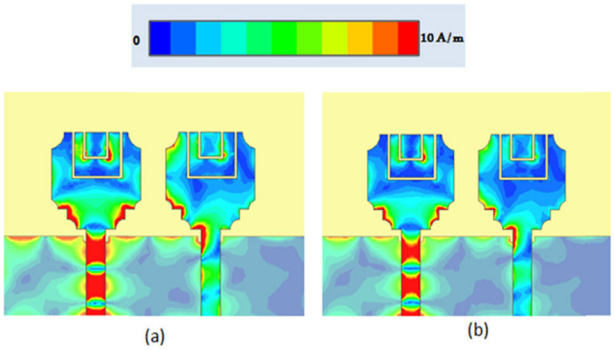

FIGURE 19. Simulated current distribution of antenna 1 at: (a) 7.8 GHz and (b) 15.3 GHz.

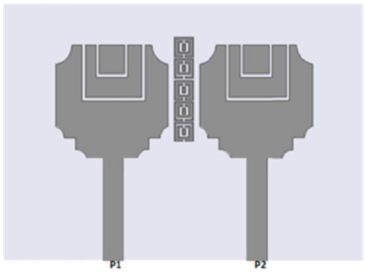

FIGURE 20. Layout of a two-antenna MIMO system with SRRs.

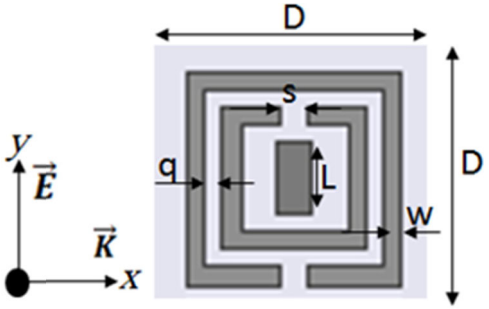

FIGURE 21. Geometry of the SRR.

dielectric substrate of the FR4-epoxy type, characterized by a dielectric constant of 4.4, a loss of 0.02 and a thickness of 1.6 mm. The square SRR studied from side (period) D = 2.4 mm, the width of the track is 0.2 mm, and the gap of two rings is 0.3 mm. The two rings are concentric and spaced 0.2mm apart. The inner ring is 1.6 mm long. Before proceeding with the simulation, a radiation box of dimensions 2.8 x 2.8 x 5.6 mm^3 was placed having electric and magnetic walls as boundary conditions. These walls must verify the excitation conditions required by the SRR. The magnetic field $\vec{H}$ must be oriented along the axis of the ring (OZ) to ensure better magnetic excitation and to circulate the induction current on the ring. For this purpose, two magnetic walls parallel to the plane (XY) and two electrical walls parallel to the plane (XZ) will be provided. The electric field $\vec{E}$ is parallel to OY to maintain a symmetrical current distribution, and the

TABLE 3. Summarizing the dimensions of the SRR cell.

Parameters	Values (mm)	Parameters	Values (mm)
S	0.3	D	2.4
Q	0.2	L	0.8
W	0.2		

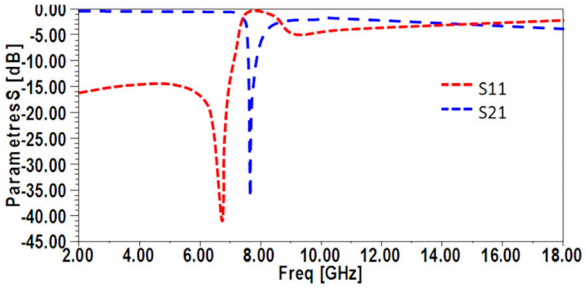

FIGURE 22. Reflection and transmission coefficients of the SRR.

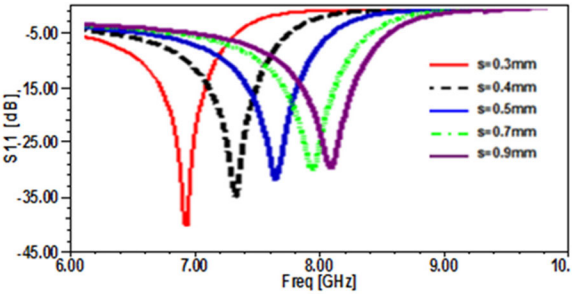

FIGURE 23. Reflection coefficient for different values of the gap in the two rings.

propagation vector $\vec{k}$ is along the OX axis. The dimensions of the SRR cell are shown in Table 3.

The simulation result of the parameters S (see figure 22) shows a resonant frequency of 7.8 GHz. The same simulation results reveal a band-cut behavior of the SRR around the 7.8 GHz frequency. An S_{11} reflection tends towards 0 dB with a much-attenuated S_{21} transmission around -35 dB. This result confirms a band gap phenomenon around the resonant frequency of the metamaterial cell; which is useful in our study to ensure better mutual decoupling in a MIMO system.

A study on the variation and influence of the size of the opening of the SRR for the two rings of the SRR is done in order to see its influence on the resonant frequency and how the latter evolves with the opening. The nominal value used is 0.3 mm and is taken as a reference. Five values are taken around the nominal value, and at the same time we keep all the other parameters fixed. The five values are: 0.3 mm, 0.4 mm, 0.5 mm, 0.7 mm and 0.9 mm. The reflection coefficient is shown in Figure 23. Figure 24 illustrates the transmission coefficient. We note that the increase in the resonant frequency is proportional to the increase in the opening.

To summarize this parametric study, we have developed table 4, which summarizes the results of all the parameters studied. In this table, we list the parameters with their values and the corresponding resonant frequencies.

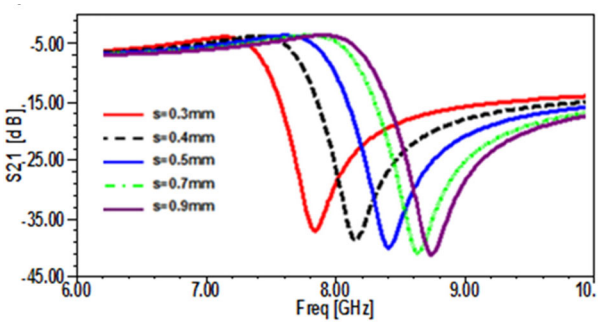

FIGURE 24. Transmission coefficient for different values of the gap in the two rings.

TABLE 4. Results summarizing the parametric study of SRR.

Parameters studied		Resonance frequency	Resonance frequency as a function of the parameter studied.
Opening size (s) of two rings: s =	0.3 mm	10.72 GHz	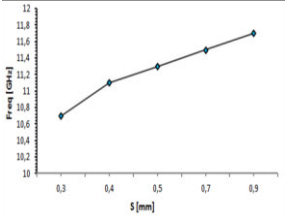
	0.4 mm	11. 12GHz	
	0.5 mm	11.33 GHz	
	0.7 mm	11.52 GHz	
	0.9 mm	11.71 GHz	
Spacing size (q) between two rings: q =	0.15 mm	10.71 GHz	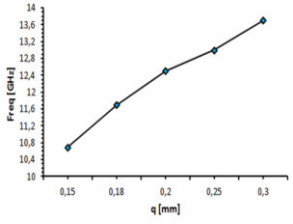
	0.18 mm	11.73 GHz	
	0.2 mm	12.51 GHz	
	0.25 mm	13.03 GHz	
	0.3 mm	13.72 GHz	
Reduced permittivity of the	2.2	13.51 GHz	
substrate: ε_r	4.4	10.71 GHz	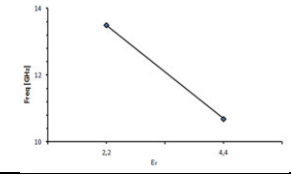

Figure 25 shows the adaptation of antenna 1 (S_{11}) and the transmission of radiation from antenna 1 to antenna 2 (S_{21}), when we have a MIMO system with and without SRRs. In simulation, we obtain an isolation gain of 27 dB at the 7.8 GHz frequency, if the SRRs are used. The transmission coefficient in this case is -43 dB versus the case without SRRs with an S21 $= -15$ dB. At this frequency we can decouple these two antennas. We also noticed that the bandwidth is extended from 2 GHz to 18 GHz, so the antenna has good adaptability over the entire operating band.

To deepen the effect of the metamaterial structure, the simulated current distributions of the antenna with and without

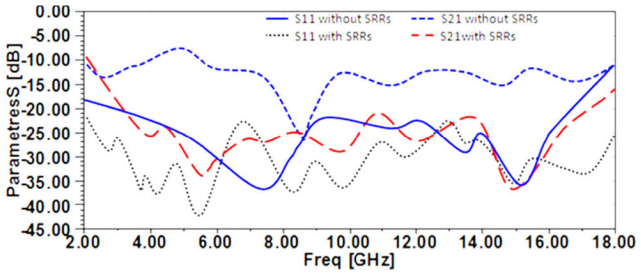

FIGURE 25. Simulation results of the S parameters with and without SRRs.

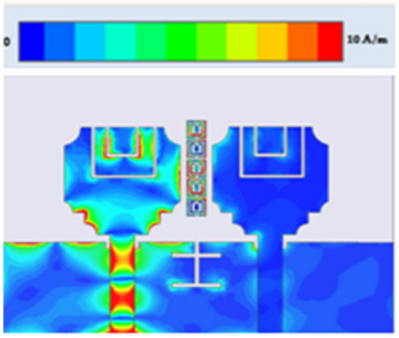

FIGURE 26. Simulated antenna current distributions with SRRs at 7.8 GHz when antenna 1 is energized.

SRRs at 7.8 GHz are illustrated in figure 26. Indeed, we can confirm that a significant isolation is ensured between the two antennas with metamaterials.

Figure 27 shows the results obtained by simulation of the ECC correlation envelope which is calculated on the basis of the parameters S according to the relation below [27]. The ECC, expressed by equation 6, is a crucial parameter to assess the diversity performance of the antenna.

$$ECC = \frac{\left|S_{11}^{*}S_{12} + S_{21}^{*}S_{22}\right|^{2}}{\left(1 - |S_{11}|^{2} - |S_{21}|^{2}\right)\left(1 - |S_{22}|^{2} - |S_{12}|^{2}\right)} \quad (6)$$

The diversity gain (DG) is a parameter that indicates in a MIMO system, whether the signal-to-noise ratio (SNR) of the combined signal is improved over the signal-to-noise ratio received by a single antenna. This parameter can be calculated using the equation 7 [27].

$$DG = 10\left(\sqrt{1 - (ECC)^{2}}\right) \quad (7)$$

As the system is symmetrical, the results of the ECC figure for port # 1 are the same as for port # 2. In the operating band, the ECC correlation envelope is very low (less than 0.1). This implies that the proposed antenna is more suitable for MIMO communications. Since the diversity gain depends to a large extent on the correlation envelope, we note from figure 27 that this gain is between 9 and 10 dB and that the maximum value is just at the point where the ECC is minimum in the operating band.

Antenna system radiation patterns are obtained when one port is powered and the other terminates with a 50 Ω load. When a port is powered, the current flow from one antenna

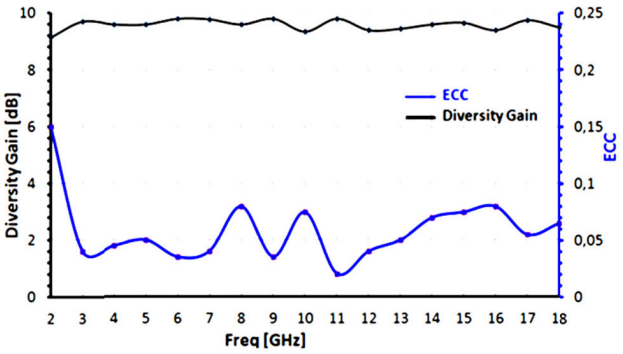

FIGURE 27. ECC and DG simulated from S parameters, for port 1 versus port 2.

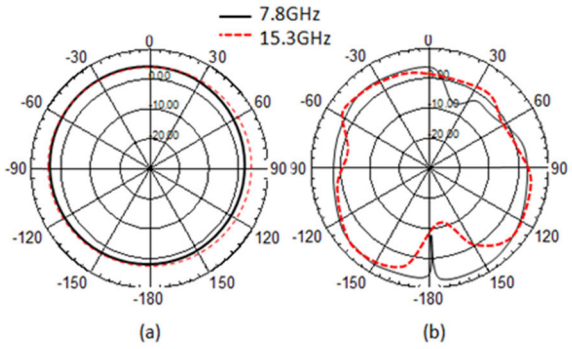

FIGURE 28. Radiation patterns of antenna 1 at frequencies: (a) 7.8 GHz and (b) 15.3 GHz.

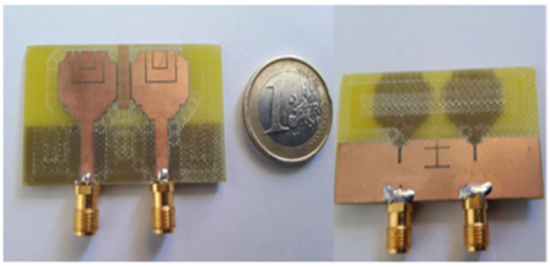

FIGURE 29. Photos of the manufactured antenna system.

element through the ground plane to the other element will be obstructed by the slotted ground plane structure and chain of SRRs. The simulated radiation patterns are shown in figure 28 for the frequencies of 7.8 GHz and 15.3 GHz in the y-z ($\phi = 90°$) and x-z ($\phi = 0°$) planes. It can be shown that the radiation patterns of the two elements are mirror transformations.

V. RESULTS OF MEASUREMENTS AND DISCUSSIONS

A prototype of the MIMO antenna described above has been manufactured and tested. Photos of the manufactured UWB MIMO antenna are shown in figure 29. The simulated and measured S-parameters of the antenna structure with and without SRRs are in good agreement, as shown in figure 30. The impedance bandwidth ($S_{11} < -10$ dB) can cover the whole of the UWB [2.1–18] GHz and the mutual coupling below −20 dB covers a large part of the UWB band.

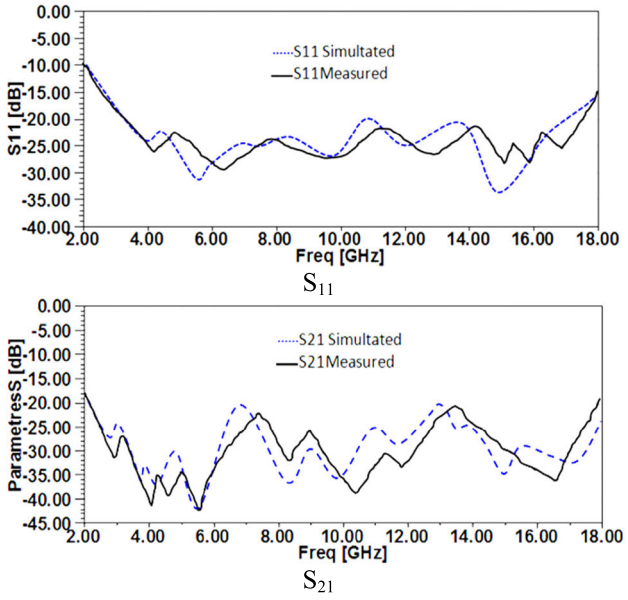

FIGURE 30. Simulated and measured S parameters of the MIMO antenna with SRRs.

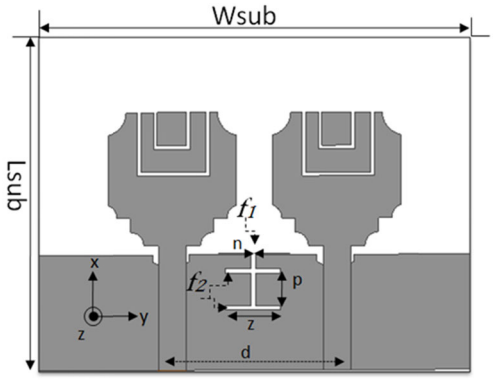

FIGURE 31. Geometry of the UWB-MIMO monopole antenna modified with the H-slot inverted.

Deviations are attributed to manufacturing tolerance and imprecise SMA connection. These results prove that this antenna is a good candidate for MIMO operation in the UWB band indicated above.

The parameters of the inverted H-type slot are optimized through a parametric study. The resulting parameters are shown in the following table:

In order to better understand the decoupling mechanism, we carried out a parametric study to analyze the impact of certain major parameters. The study is based on the antenna geometry given in figure 31. The results of the research are presented in figures 32 and 33. First of all, the width 'n' varies from 0.2 to 0.8 mm while the other parameters are not changed. Its effects on the S parameters (| S11 | and | S21 |) are shown in figure 32. It is clearly seen that by increasing the width 'n' from 0.2 to 0.8 mm, the simulated S parameters (reflection coefficient S11 and transmission coefficient S21) are significantly affected; that is, the bandwidth for | S11 | < -10 dB is reduced from (2.3-18) GHz to (4.7-16) GHz

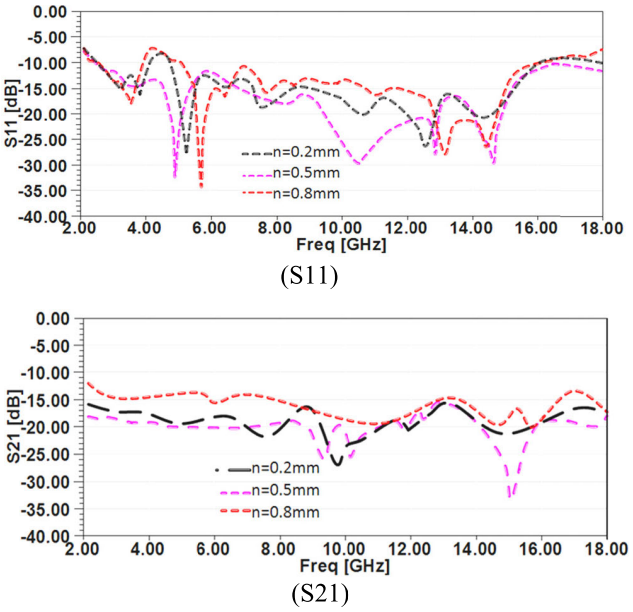

FIGURE 32. Simulated S parameters of antenna 2 for different values of 'n'.

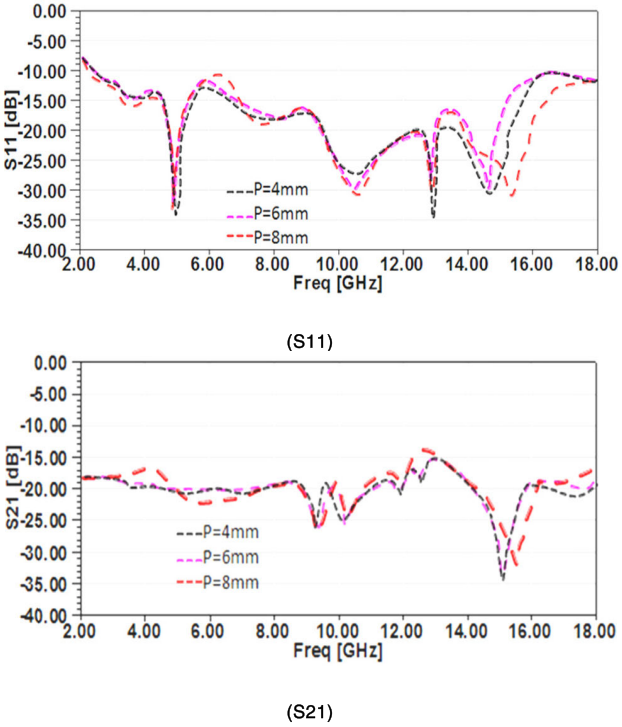

FIGURE 33. Simulated S parameters of antenna 2 for different 'p' values.

and the decoupling bandwidth for | S21 | < -15 dB is reduced from (2.3-17.5) GHz to (8-16.3) GHz, as shown in figures 32.a and 32.b respectively. The major impact seems to be at lower frequencies (around 4.2 GHz), especially on S11. This is understandable, since the electrical length of the ground plane is small.

Second, the effect of the parameter 'P', which determines the length of slot 1 on antenna 2, is studied. When the length

TABLE 5. Dimensions of the proposal Inverted H-Type with the DGS technique.

Parameters	n	p	z	d	Wsub	Lsub
Valus (mm)	0.5	6	6	16.8	48	35

TABLE 6. Summary of the influence of the slot parameters (mm) on the S parameter.

Parameters (mm)		bandwidth (GHz) (S11 <-10 dB)	bandwidth (GHz) (S21 <-15 dB)
n	0.2	4.7-16	2-18
	0.5	2.3-18	2-18
	0.8	5.2-16	8-16.2
p	4	2.4-16.1	2-18
	6	2.3-18	2-18
	8	2.4-16.2	2-12.1
z	4	2.3-14.5	2.3-16.4
	6	2.3-18	2-18
	8	2.2-17.8	3.6-17.3

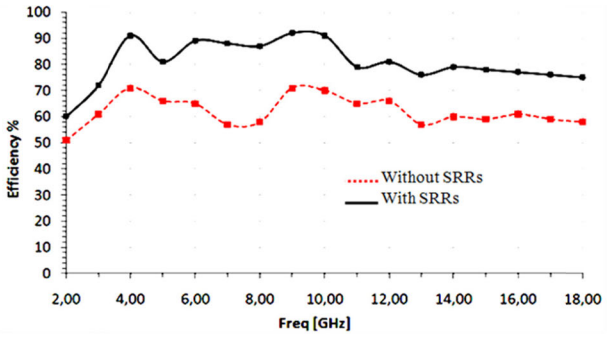

FIGURE 34. Total efficiency of simulated antenna 1 with and without SRRs.

'P' is increased from 4 to 8 mm, the decoupling slot lengthens; this has little impact on the bandwidth ($|S11| < -10$ dB), as shown in figure 33. However, a slight modification will affect the transmission coefficient | S21 |. When the length P = 8 mm, the bandwidth of the coupling will be affected, more precisely, will affect the sub-band from 12.3 to 13 GHz.

Finally, the effects of all the other parameters of the slits are studied. Similar performance can also be seen when the length of the slit 'z' is increased from 4 to 8 mm. The effects of the slots on the antenna S parameters are summarized in Table 6.

It emerges from the above analysis that the width of the strip is less sensitive to the length and width of the slot than the coupling coefficient. The optimal values of n, p and z are respectively 0.5, 6 and 6 mm.

In figure 34, we notice that the simulated efficiency of a single antenna put in MIMO system without application of SRRs is between 57 and 73% over the whole operating band. The maximum total efficiencies of the different antennas in the reference system are not very high because of the coupling between these antennas. As expected, increasing the isolation between the antennas improves their overall efficiencies. Therefore, the transmission rate increases. According to figures 32, the minimum value of the insulation is −44 dB which

TABLE 7. Comparison among the presented MIMO antenna and the previously reported Band-Notched UWB-MIMO antennas.

No.	Ref.	Element Number	Bandwidth (GHz)	Dimensions (mm× mm)	Gain (dBi)	Radiation Efficiency (%)	ECC
1	[21]	1	3.1–17.5	65 x 65	6	-----	-----
2	[22]	1	2–16	50 x 30	3.5–6	80	<0,2
3	[29]	4	2.95–10.8	44 x 44	2-6	78	<0.1
4	[30]	4	5–6	60 x 32	7.5	85	<0.04
5	Proposed Antenna	2	2-18	48 x 35	2-8	85	<0,07

seems interesting to have a good total efficiency. We can clearly see on the curve of figure 32, that the total efficiencies of the MIMO system with insertion of SRRs are higher than those of the system without SRRs and that in the entire desired operating band. In the best case, the absolute benefit in% provided by the isolation technique applied with the use of SRRs on the total efficiency is + 20%. Table 7 shows the comparison of the UWB MIMO antenna with other UWB MIMO antennas existing in the literature. From this table it is concluded that the designed antenna has many advantages over the antennas of [21], [22] and [14], [28], in terms of size, bandwidth and inter-element isolation.

VI. CONCLUSION

In this paper, the studies and research that have been discussed have focused on the design, optimization and performance evaluation of two element MIMO systems based on metamaterials for communication networks applied to antennas UWB. The simulation results of the final system developed confirmed the advantages of the proposed idea not only from the point of view of mutual coupling but also in terms of weight reduction, size and gain in diversity. The suggested antenna presents a good diversity performance with ECC < 0.1 and diversity gain (DG > 9 dB) and the efficiency is around 89%. This is beneficial for their integration into telecommunications systems.

REFERENCES

[1] *First Order and Report, Revision of Part 15 of the Commission's Rules Regarding UWB Transmission Systems*, document FCC 02-48, Federal Communications Commission, Apr. 2002.

[2] G. Gao, B. Hu, L. He, S. Wang, and C. Yang, "Investigation of a reconfigurable dual notched UWB antenna by conceptual circuit model and time-domain characteristics," *Microw. Opt. Technol. Lett.*, vol. 59, no. 6, pp. 1326–1332, Jun. 2017.

[3] R. B. Rani and S. K. Pandey, "A CPW-fed circular patch antenna inspired by reduced ground plane and CSRR slot for UWB applications with notch band," *Microw. Opt. Technol. Lett.*, vol. 59, no. 4, pp. 745–749, Apr. 2017.

[4] M. S. Sharawi, S. K. Podilchak, M. T. Hussain, and Y. M. M. Antar, "Dielectric resonator based MIMO antenna system enabling millimetre-wave mobile devices," *IET Microw., Antennas Propag.*, vol. 11, no. 2, pp. 287–293, Jan. 2017.

[5] W. Xiao, T. Mei, Y. Lan, Y. Wu, R. Xu, and Y. Xu, "Triple band-notched UWB monopole antenna on ultra-thin liquid crystal polymer based on ESCSRR," *Electron. Lett.*, vol. 53, no. 2, pp. 57–58, Jan. 2017.
[6] C. Sabah and T. Nesimoglu, "Design and characterization of a resonator-based metamaterial and its sensor application using microstrip technology," *Opt. Eng.*, vol. 55, no. 2, Feb. 2016, Art. no. 027107.
[7] S. S. Al-Bawri, M. S. Islam, H. Y. Wong, M. F. Jamlos, A. Narbudowicz, M. Jusoh, T. Sabapathy, and M. T. Islam, "Metamaterial cell-based superstrate towards bandwidth and gain enhancement of quad-band CPW-fed antenna for wireless applications," *Sensors*, vol. 20, no. 2, pp. 1–14, 2020.
[8] A. Iqbal, O. A. Saraereh, A. W. Ahmad, and S. Bashir, "Mutual coupling reduction using F-shaped stubs in UWB-MIMO antenna," *IEEE Access*, vol. 6, pp. 2755–2759, 2018.
[9] J. Ghosh, S. Ghosal, D. Mitra, and S. R. B. Chaudhuri, "Mutual coupling reduction between closely placed microstrip patch antenna using meander line resonator," *Prog. Electromagn. Res. Lett.*, vol. 59, pp. 115–122, 2016.
[10] S. Zhang, B. K. Lau, A. Sunesson, and S. He, "Closely-packed UWB MIMO/diversity antenna with different patterns and polarizations for USB dongle applications," *IEEE Trans. Antennas Propag.*, vol. 60, no. 9, pp. 4372–4380, Sep. 2012.
[11] A. Suntives and R. Abhari, "Miniaturization and isolation improvement of a multiple-patch antenna system using electromagnetic bandgap structures," *Microw. Opt. Technol. Lett.*, vol. 55, no. 7, pp. 1609–1612, Jul. 2013.
[12] F. G. Zhu, J. D. Xu, and Q. Xu, "Reduction of mutual coupling between closely-packed antenna elements using defected ground structure," *Electron. Lett.*, vol. 45, no. 12, pp. 601–602, 2012.
[13] G. Adamiuk, S. Beer, W. Wiesbeck, and T. Zwick, "Dual-orthogonal polarized antenna for UWB-IR technology," *IEEE Antennas Wireless Propag. Lett.*, vol. 8, pp. 981–984, 2009.
[14] M. Saeed Khan, A.-D. Capobianco, S. M. Asif, D. E. Anagnostou, R. M. Shubair, and B. D. Braaten, "A compact CSRR-enabled UWB diversity antenna," *IEEE Antennas Wireless Propag. Lett.*, vol. 16, pp. 808–812, 2017.
[15] A. K. Verma, R. Nakkeeran, and R. K. Vardhan, "Design of 2 × 2 single sided wrench shaped UWB MIMO antenna with high isolation," in *Proc. Int. Conf. Circuit, Power Comput. Technol. (ICCPCT)*, Mar. 2016, pp. 18–19.
[16] A. Toktas, "G-shaped band-notched ultra-wideband MIMO antenna system for mobile terminals," *IET Microw., Antennas Propag.*, vol. 11, no. 5, pp. 718–725, Apr. 2017.
[17] J. Tao and Q. Feng, "Compact UWB band-notch MIMO antenna with embedded antenna element for improved band notch filtering," *Prog. Electromagn. Res. C*, vol. 67, pp. 117–125, 2016.
[18] L. Liu, S. W. Cheung, and T. I. Yuk, "Compact MIMO antenna for portable UWB applications with band-notched characteristic," *IEEE Trans. Antennas Propag.*, vol. 63, no. 5, pp. 1917–1924, May 2015.
[19] P. Gao, S. He, X. Wei, Z. Xu, N. Wang, and Y. Zheng, "Compact printed UWB diversity slot antenna with 5.5-GHz band-notched characteristics," *IEEE Antennas Wireless Propag. Lett.*, vol. 13, pp. 376–379, 2014.
[20] W. T. Li, Y. Q. Hei, H. Subbaraman, X. W. Shi, and R. T. Chen, "Novel printed filtenna with dual notches and good Out-of-Band characteristics for UWB-MIMO applications," *IEEE Microw. Wireless Compon. Lett.*, vol. 26, no. 10, pp. 765–767, Oct. 2016.
[21] Y.-Y. Liu and Z.-H. Tu, "Compact differential band-notched stepped-slot UWB-MIMO antenna with common-mode suppression," *IEEE Antennas Wireless Propag. Lett.*, vol. 16, pp. 593–596, 2017.
[22] W. Wu, B. Yuan, and A. Wu, "A quad-element UWB-MIMO antenna with band-notch and reduced mutual coupling based on EBG structures," *Int. J. Antennas Propag.*, vol. 2018, pp. 1–10, Feb. 2018.
[23] N. K. Kiem, H. N. B. Phuong, and D. N. Chien, "Design of compact 4 × 4 UWB-MIMO antenna with WLAN band rejection," *Int. J. Antennas Propag.*, vol. 2014, Jul. 2014, Art. no. 539094.
[24] V. S. D. Rekha, P. Pardhasaradhi, B. T. P. Madhav, and Y. U. Devi, "Dual band notched orthogonal 4-element MIMO antenna with isolation for UWB applications," *IEEE Access*, vol. 8, pp. 145871–145880, 2020.
[25] K.-L. Wong, Y.-C. Chen, and W.-Y. Li, "Four LTE low-band smartphone antennas and their MIMO performance with user's hand presence," *Microw. Opt. Technol. Lett.*, vol. 58, no. 9, pp. 2046–2052, Sep. 2016.
[26] J. Choi, W. Hwang, C. You, B. Jung, and W. Hong, "Four-element reconfigurable coupled loop MIMO antenna featuring LTE full-band operation for metallic-rimmed smartphone," *IEEE Trans. Antennas Propag.*, vol. 67, no. 1, pp. 99–107, Jan. 2019.
[27] S. Blanch, J. Romeu, and I. Corbella, "Exact representation of antenna system diversity performance from input parameter description," *Electron. Lett.*, vol. 39, no. 9, pp. 705–707, May 2003.
[28] R. Mark, N. Rajak, K. Mandal, and S. Das, "Metamaterial based superstrate towards the isolation and gain enhancement of MIMO antenna for WLAN application," *AEU, Int. J. Electron. Commun.*, vol. 100, pp. 144–152, Feb. 2019.

HEDI SAKLI was born in Tunisia, in 1966. He received the M.S. degree in high-frequency communication systems from Marne-La-Valley University, France, in 2002, and the Ph.D. and H.D.R. degrees in telecommunications from the National Engineering School of Tunis, Tunis El Manar University, Tunisia, in 2009 and 2014, respectively.

Since 2010, he has been an Assistant Professor with the University of Gabes, where he was an Associate Professor, in 2017. He is the author of more than 60 articles. His research interests include propagation in anisotropic media, ferrite and metamaterials, numerical methods in electromagnetic, FSS, antennas, sensors, 5G, connected objects, sensor networks, and artificial intelligence.

C. ABDELHAMID was born in Tunisia, in 1978. He is currently a Research Engineer in microwave engineering with the Center for Studies and Research of Telecommunications (CERT). He is the author of ten articles. His research interests include RF and microwave, design of hybrid active and passive monolithic microwave circuits, metamaterials, and miniature antennas.

C. ESSID was born in Kef, Tunisia, in March 1979. He received the degree in mathematics from the Faculty of Science of Tunisia, in 2001, and the M.Sc. degree in communication systems and the Ph.D. degree in telecommunications (microwave engineering) from the National Engineering School of Tunis (ENIT), Tunis El Manar University, Tunisia, in 2003 and 2010, respectively.

He is currently an Assistant Professor with the Faculty of Science and a member of the SERCOM Laboratory, Tunisia Polytechnic School, Carthage University. He is the author of more than 15 articles. His current research interests include microwave, antennas and propagations, 5G, and sensors.

N. SAKLI was born in Tunisia, in 1981. He is the President of EITA Consulting, Paris, France. He is the author of seven articles. His research interests include computer science, 5G, deep learning, connected objects, the IoT, and sensor networks.